Powder Processing and Densification Behaviour of Alumina – High Zirconia Nanocomposites Using Chloride Precursors

Raghunath P. Rana, Swadesh K. Pratihar* and Santanu. Bhattacharyya
Department of Ceramic Engineering
National Institute of Technology, Rourkela – 769008, India
*author for correspondence

_____

Abstract:

Al_2O_3-ZrO_2 composites having nominal equal volume fraction of Al_2O_3 and ZrO_2 were prepared from gel-precipitated powder, precipitated powder and washed precipitated powder. These different processing routes affected the crystallization temperature of the amorphous powders as well as the phase evolution of Al_2O_3 and ZrO_2 during calcination. The agglomerate size was largest for gel-precipitated powder (30 μm) and it was smallest for washed precipitated powder (19 μm). While gel-precipitated powder produce hard agglomerated powders (Pj=110 MPa), washed precipitated powders produce soft agglomerates with low agglomeration strength (Pj=70MPa). Thus washed precipitated powders could sinter to a high density at lower sintering temperature. The bending strength exhibits a semi-logarithmic relationship with porosity. The hardness shows an increasing trend with sintering temperature.

Keywords: - Al_2O_3-ZrO_2; Nanocomposites; Processing; Agglomerates; Bending strength

_____

* Corresponding author: Tel: +91 661246 2206; Fax: +91 661 247 2926

E-mail: skpratihar@nitrkl.ac.in

1. Introduction

Alumina-Zirconia composite is an important class of toughened structural ceramic in which the strength and toughness have been improved due to stress induced t-m transformation [1-3]. The extent of toughening achieved in this composite depend on the particle size of Al_2O_3 and ZrO_2, volume fraction of ZrO_2 retained in the metastable tetragonal phase as well as on the relative distribution of Al_2O_3 and ZrO_2 in the matrix [4]. While a finer particle size of both Al_2O_3 and ZrO_2 will not only enhance the chances of a uniform Al_2O_3 and ZrO_2 distribution, it also increases the possibility of ZrO_2 being retained as metastable tetragonal phase [5]. A major problem in achieving a high density $Al_2O_3 - ZrO_2$ composites is the coarsening of ZrO_2 particles during high temperature processing [6]. The coarsening of ZrO_2 will not only adversely affect the densification behaviour but also will reduce the retained tetragonal ZrO_2. Thus efforts are being made to prepare ultrafine particles of Al_2O_3 and ZrO_2 through different improved processing routes like sol-gel [7], combustion synthesis [8], precipitation [9], gel-precipitation [10] etc. The specific advantages of these ultrafine powders are superior phase homogeneity and low temperature sinterability. A uniform powder shape having a continuous and narrow size distribution are expected to yield products with reduced microstructural defects due to improved powder flowability and better packing density. The improved densification at a relatively low temperature is only possible for uniform and high density packing. These features can only be achieved if the powder remains in the unagglomerated state. Hard agglomerates of chemical processed powders (particle size less than 1 μm) result from the development of strong hydrogen bond during the post

processing high temperature calcination of the powder. Once the ultrafine powders are agglomerated, the agglomerate strength becomes quite high so that the realistic benefit of the using ultrafine powders having nano-sized crystallites are not realized. The weaker bonding between particles produces soft agglomerates, which have good flowability and compaction behaviour. Although in the recent past a major research interest in the field of powder processing science has been minimized of these hard agglomerates [11-15], the characterization of the powders particularly that of agglomeration behaviour due to a change in the powder processing parameter as well as post powder processing treatment has not been studied in detail. Two important characteristics, which can affect the densification behaviour of these ultrafine powders, are agglomerate strength and agglomerate size. However, only few reports are available on the powder processing and characterization of Al_2O_3-ZrO_2 composite powder having nominally equally volume fraction of Al_2O_3 and ZrO_2. In this paper, we report the effect of powder processing technique as well as the post powder processing treatment on the phase evolution, agglomerate strength, agglomerate size, densification behaviour, strength and hardness of Al_2O_3-ZrO_2 composites containing nominally equally volume fraction of Al_2O_3 and ZrO_2.

2. Experimental

Al_2O_3-ZrO_2 composites were prepared from analytical reagent grade $ZrOCl_2.8H_2O$ and $AlCl_3$. Three different processing routes were adopted for powder processing viz. Gel-Precipitation (GPT) route, Precipitation (PPT) route, and Washed Precipitation (WPT) route. In all the three routes, the precipitation was affected by addition of 1:1 solution of analytical reagent grade NH_4OH. While the pH was maintained between 6-6.5 for GPT route, it was in the range of 8.7-9.1 for the other two

routes. In the PPT route, the precipitate of Al and Zr were allowed to settle till a clear supernatant liquid was obtained. Subsequently, the supernatant liquid was drained off and the precipitated powder was dried. Further in the WPT route powders, the precipitates were also washed with hot water and alcohol prior to calcination. Details of the powder preparation by these routes have been reported earlier [16]. All the three type of hydrated samples were dried in an oven at about 80^0C and grounded to a fine powder. The thermal decomposition behaviour of the powders till 1250^0C was studied by DSC/TG at a heating rate of 10^0C/min (NETZSCH STA). The powders were calcined at different temperatures (350^0C -950^0C) to study the phase evolution by X-ray diffraction technique (Philips 1830, Netherland). Crystallite size of all the three varieties of calcined powder was determined from the X-ray line broadening technique using Scherrer formula [17]. The agglomerate size and distribution of the calcined GPT, PPT, and WPT powder was measured by laser scattering technique (Malvern MASTER SIZER, U.K.).   A small amount of calcined powder of each of the three varieties was compacted in an UTM (Hounsfield H50KT, UK) at a constant crosshead speed of 0.2mm/min to study the compaction behaviour and agglomerate strength of the powders. The constant rate heating sintering behaviour of the powder compacts was studied in a dilatometer (NETZSCH 402C) at the heating rate of 5^0C/minute. Green compacts of the above three powder prepared by uniaxial pressing were sintered in air in the temperature range 1400^0-1600^0C with a holding time of 4 hours at the peak temperature. The sintered density of the samples was measured by Archimedes's principle using kerosene as immersion liquid. The hardness of the sintered WPT samples was measured by Vickers Hardness Tester (Blue Star Limited, VM-50, India). The bending strength of sintered WPT samples

were measured in an UTM (Hounsfiled H10KT, UK) by Brazilian Disc Test methods on the cylindrical samples of 12.5 mm diameter. Corresponding to each sintering temperature, a set of five samples was tested. The bending strength was calculated from the formula [18].

$$\sigma = \frac{2P}{\pi Dt} \qquad (1)$$

where, P is the breaking load, D is the diameter of the pellet and t is the thickness of the pellet.
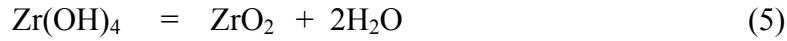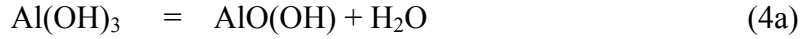
3. Results & Discussions

3.1 Thermal Analysis

Fig.1 (a) shows the DSC/TG plot of GPT powder. The curve shows three endothermic peaks at 105^0C, 185^0C and 310^0C respectively. The endothermic peak at 105^0C has a rather broad nature covering a temperature range of 40^0C-175^0C. In contrast the other two peaks (i.e. at 185^0C and 310^0C) are quite sharp. The TG curve on the other hand, shows total weight loss of about 68%, which takes place in four stages. In the first stage (30^0C-100^0C), the weight loss is about 8.0%. The second stage of weight loss occurring in the temperature range (100^0C -190^0C) is about 5%. The third stage of weight loss (40%) is observed between 200^0C -309^0C. The final stage of weight loss (12%) takes place in the temperature range of 320-450^0C. A broad exothermic peak is also observed in the temperature range 450^0C-500^0C. The weight loss sequence during the decomposition and crystallization of precipitated amorphous hydroxides in could be explained by considering the following chemical reactions of $AlCl_3$ and $ZrOCl_2$ with NH_4OH.

$$AlCl_3 + NH_4OH = Al(OH)_3 + 3NH_4Cl \qquad (2)$$

$$ZrOCl_2 + NH_4OH + H_2O \ = \ Zr(OH)_4 + 2NH_4Cl \qquad (3)$$
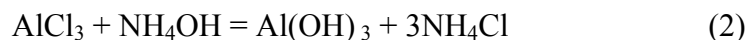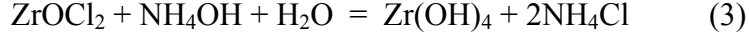
According to the Eqns. (1) and (2) for equal volume fraction of Al_2O_3 and ZrO_2 the total weight loss for the decomposition of NH_4Cl will be about 48%.

The other product on the RHS of Eqns. (2) and (3), i.e., $Al(OH)_3$ and $Zr(OH)_4$, decomposes according to the following chemical reactions:

$$Al(OH)_3 \ = \ AlO(OH) + H_2O \qquad\qquad (4a)$$

$$2AlO(OH) = \ Al_2O_3 + \ H_2O \qquad\qquad (4b)$$

$$Zr(OH)_4 \ = \ ZrO_2 \ + \ 2H_2O \qquad\qquad (5)$$

Thus the decomposition of $Al(OH)_3$ is a two step process [Eqn. 4(a) and 4 (b)] involving a weight loss of 9 and 5.8% respectively. On the other hand, the decomposition of $Zr(OH)_4$ is a single step process involving a weight loss of 13.89% [Eqn. (5)]. Therefore, in the light of the above discussion, it can be said that the first two endothermic peaks at 105^0C and 198^0C respectively and the associated weight losses of 8 and 5% respectively in the temperature range 30^0C -220^0C are due to the dehydroxylation of $Al(OH)_3$ to Al_2O_3. The decomposition of NH_4Cl takes place in the temperature range of 290^0C-300^0C. Thus the endothermic peak at 309^0C associated with the weight loss of 40% could be assigned to the combined weight loss for NH_4Cl reaction [Eqns. (2) and (3)]. The remaining weight loss of 12% in the temperature range 320-400^0C could be attributed to the decomposition of $Zr(OH)_4$. The difference in the observed and theoretical weight loss could be because of GPT technique. As already mentioned the pH at the point of gelation was between 6-6.5. Under this situation, complete precipitation of all the chloride ions of Al and Zr as NH_4Cl does not happen prior to gelation. Thus a part of both $AlCl_3$ and $ZrOCl_2$ remain entrapped in the gel network and

thus the actual amount of $Al(OH)_3$ and $Zr(OH)_4$ available for decomposition (in accordance with the above reaction) becomes less than the theoretical value. It appears that the endothermic peak corresponding to the decomposition of $Zr(OH)_4$ has been masked by the very strong endothermic peak for NH_4Cl decomposition.

The DSC/TG plot of PPT powder [Fig.1 (b)] shows a nature, which is different from that of GPT powder. The DSC/TG curve have only two endothermic peak, the first one is a broad one which is spread over a temperature range 30^0C-180^0C followed by a second endothermic peak at 290^0C.The TG curve shows that the total weight loss of 52% takes place in three stages. The first stage involves a weight loss is 14% taking place upto about 180^0C.The second stage of weight loss is about 24% observed between 180^0C-320^0C and the third and final stage of weight loss (13%) is observed between 320^0C-350^0C. The reactions that led to DSC peaks and the TG weight losses are according to the Eqns. (2) to (5). Thus the first endothermic peak and the associated weight loss correspond to the dehydroxylation of $Al(OH)_3$. The second endothermic peak and the associated weight loss is due to the decomposition of NH_4Cl and the third stage weight loss relate to the dehydroxylation of $Zr(OH)_4$. However since the PPT powders were prepared at a much higher pH (8.7-9.1), complete precipitation of both $AlCl_3$ and $ZrOCl_2$ took place. Thus the observed weight loss for the dehydroxylation of $Al(OH)_3$ and $Zr(OH)_4$ matches with that of theoretical value. The lower observed weight loss for the decomposition of NH_4Cl is probably due to the partial removal of NH_4Cl through dissolution in excess water. Moreover it is observed that the dehydroxylation of $Al(OH)_3$ in PPT powder is a single step process, instead of two stage dehydroxylation of GPT powder according to the reaction.

$$2Al(OH)_3 = Al_2O_3 + 3H_2O \qquad (6)$$
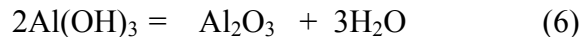
The DSC/TG plot of WPT powder is shown in Fig.1 (c). The DSC curve in this case shows only one broad endothermic peak around 105^0C followed by two overlapping exothermic peak at 275^0C and 300^0C. At still higher temperature another broad exothermic peak is observed at 875^0C. The TG plot on the other hand shows a total weight loss of 28.6% which takes place in two steps. In the first step, the single stage decomposition of $Al(OH)_3$ takes place to Al_2O_3 according to the reaction (6).

The theoretical weight loss for this reaction is 13.5% for equal volume fraction Al_2O_3 and ZrO_2. The observed weight loss is about 14%, which matches the theoretical value. The second stage of weight loss starts from about 200^0C and continues till 600^0C. The weight loss in this stage is 14%, which agrees well with the theoretical weight loss of 13.89% for dehydroxylation of $Zr(OH)_4$. The first of the two exothermic peaks, which appear at 275^0C, could be due to crystallization of $\gamma-Al_2O_3$ from Boehmite $(Al(OH)_3)$. The second exothermic peak at 300^0C could be because of crystallization of cubic-ZrO_2 from $Zr(OH)_4$. Finally the broad exothermic peak around 875^0C could be due to the phase transformation of cubic-ZrO_2 to tetragonal ZrO_2.

3.2 Phase Analysis

The sequence of phase evolution with calcination temperature is shown Fig. 2-4 for all the three types of powders. Fig. 2 shows the XRD pattern of GPT powders calcined at different temperatures. In the temperature range 350^0C-550^0C, only a few broad peaks corresponding to cubic ZrO_2 (JCPDS File 81-1550) appears with an

additional peak is observed having d spacing 2.80 A^0 was observed. The broad peak of cubic zirconia indicates that the powder has very fine crystallites (15.3 nm measured by x-ray line broadening). The additional peak at d spacing 2.80 A^0 matches well with that of $AlCl_3$ and $ZrOCl_2$ (JCPDS File 77-0819 and 76-1575 respectively). This peak disappears on calcining the powder at 550^0C and above. During calcination, the entrapped $AlCl_3$ and $ZrOCl_2$ directly decompose to Al_2O_3 and ZrO_2 respectively. This supports the decomposition behaviour of the GPT powder explained earlier. At higher temperature 750^0C, the tetragonal ZrO_2 also starts appearing along with cubic-ZrO_2. At 850^0C, only tetragonal ZrO_2 is present. At 950^0C, both monoclinic and tetragonal ZrO_2 is present and the monoclinic ZrO_2 present was 21 vol%. The amount of monoclinic ZrO_2 was calculated from the intensity ratio of tetragonal and monoclinic ZrO_2 using Schmid's formula [19]. The phase transformation observed in ZrO_2 (amorphous$\rightarrow$ cubic$\rightarrow$ tetragonal$\rightarrow$ monoclinic) follows Garvie theory [5]. In PPT powders (Fig.3), the phase changes follow the same sequence as that of GPT powder. However, in PPT powders no monoclinic ZrO_2 could be observed even at 950^0C. This could be due to the lower crystallite size of PPT powders. However, no peaks of alumina could be detected in either GPT or PPT powders. This could be due to the lower atomic scattering factors of transition alumina phases. Fig.4 shows the XRD pattern of WPT powder. It may be noted that the XRD pattern of WPT powder starts from 650^0C instead of 350^0C as observed for the other two powders. The reason for this being the powder remained amorphous at lower temperature. The low temperature crystallization of GPT and PPT powders could be due to the presence of chloride ions in the powder. It has been observed that chlorides affect the crystallization temperatures and phases of amorphous Al and Zr hydroxides

[20]. Since only a trace amount of chloride was present in WPT powder, the crystallization was shifted to a higher temperature. Thus washing of precipitated powders by hot water and propanol prior to calcination produces very fine powders, which helps to retain tetragonal ZrO_2 even at 950^0C. Thus, the crystallite size of GPT, PPT and WPT powders are 15.3 nm, 12.8 nm and 7.50 nm respectively. The crystallite size value shows that among the three types of powders, WPT has the finest crystallite size of ZrO_2.

3.3 Particle size Analysis

The particle size frequency distribution of calcined GPT, PPT and WPT powders is shown in Fig.5. The figure clearly shows the effect of processing route on the particle size and its distribution. While GPT powders show that the majority of the particles are in the size range of 30-50 µm with very few particles on the lower size (<10 µm) on the other hand, PPT powders show that the population of lower size fraction marginally increases to a higher value. Finally in WPT powders, the volume fraction of large size particles decreases while that of small particle size (<10 µm) increases. Thus hot water and propanol washing of the precipitated powders prior to calcination produces much finer particle with wide size distribution and a smaller average particle size. Thus WPT powder is expected to produce compacts with good green density and consequently higher sintered density.

3.4 Compaction behaviour of powders

Fig.6 shows the semi logarithmic plot of compaction pressure vs. density of green compacts for GPT, PPT and WPT powders. All the three kinds of powders show that the compaction response diagram has two segments, viz. low pressure and high-pressure zone. At low compaction pressure the green density is low and green density increases

rapidly beyond a critical pressure. In the low pressure range, densification proceeds by fragmentation and rearrangement of the agglomerates without the occurrence of compression of their internal structure. In the high pressure range densification continues by compression and consequently densification of the internal agglomerates. The critical pressure is found out from the intersection of the two tangents for the two segments. The critical pressure (Pj) is called the agglomerate break point and it denotes the strength of the agglomerate. The lower is the agglomerate strength the better will be the compaction of the powder. From the figure the Pj value for GPT, PPT and WPT powders are found to be 110, 97 and 70 MPa respectively. Thus the GPT powders produces rather strong agglomerates while WPT produce weak agglomerates due to post precipitation powder treatment of hot water and propanol washing.

The graph of green density vs ln (compaction pressure) provides important information about the powder compaction behaviour. Usually, for chemically processed powders two stage compaction behaviour is observed:

  Stage-I   Granule flow and rearrangement

  Stage-II   Granules deformation combined with granule densification.

Stage-I take place at lower pressure and is associated with small amount of sliding and granule rearrangement. Stage-II occurs above P_j and begins with granule deformation which subsequently shifts to granule densification process. The dependence of agglomerate break point P_j on the granule parameter during stage –II compaction can be described by the equation [21]:

$$\rho_{compact} = \rho_{fill} + m\log\frac{P_a}{P_j} \qquad (7)$$

Where $\rho_{compact}$ is the compact density at an applied pressure P_a, ρ_{fill} is the filled density and m is the compaction constant that depends on the deformability and densification characteristics of the granules.

It is usually observed that powder containing high density granules usually produce a high compact density with a lower value of m (up to 5%). Softer or low density granules, on the other hand produce m value in the range 7-10 %. In the present study, the m value obtained using Eqn. (7) is 2.2, 2.6 and 3% for GPT, PPT and WPT powder respectively. Thus all powders have high density granules, but the WPT powder has relatively softer granules. Thus washing of powders seems to have an effect on the compaction behaviour of powders.

3.5 Sintering Behaviour and Density of Compacts

The constant rate heating densification behaviour of GPT, PPT and WPT powders is shown in Fig.7. All the three types of compacts show that shrinkage starts in the range 950-1000^{0}C and all of them exhibit two-stage densification behaviour. The second stage of the densification starts in the temperature range 1260-1280^{0}C. Similar observations in the densification behaviour have been observed by others working with Al_2O_3-high ZrO_2 system [22]. The detailed analysis of the densification behaviour for these compacts will be reported separately. However, the present curve shows that there is a difference in the shrinkage behaviour of GPT, PPT and WPT compacts. While the first two powders show shrinkage of only 8% at the end of first stage, WPT samples shows shrinkage of 20% at the end of first stage. An initial finer particle size leads to a higher sintered density on account of higher reactivity of WPT powders. The reactivity of the powders depends on

specific surface area and particle size. The specific surface area of WPT powder is 123 m^2/gm, which is much higher in comparison to other two viz. GPT (49 m^2/gm) and PPT (71 m^2/gm) powders. The higher specific surface area means a finer particle size, which is 20 nm for WPT 51, 41 nm for PPT and nm for GPT. Thus WPT powders are more reactive. This indicates that WPT powders are much finer and is more reactive and thus it will densify to a higher density at a lower temperature.

Fig.8 shows the relative density of the sintered compacts as a function of sintering temperature for all the three type of compacts, viz. GPT, PPT and WPT. All the three type of compacts shows an increase in the sintered density with increasing sintering temperature. However, both GPT and PPT compacts show similar trend in the density increments and both the compacts have comparable densities till about 1550^0C. Only at 1600^0C, the densities of GPT and PPT compacts vary widely. This difference in sintering behaviour could be correlated with their powder characteristics. GPT powders have strong and large agglomerate (Pj = 106 MPa, $D_{0.5}$ = 35 μm) which probably results in localized and differential sintering leading to a poor sintered density.

On the other hand, the variation of relative density against sintering temperature for compacts prepared from WPT powders shows a different behaviour. These samples show a high relative density (>71%) even at 1400^0C due to wide particle size distribution. However, the increase in relative density with increasing sintering temperature is rather small and at 1600^0C only 89% relative density is achieved. The small increase in sintered density of WPT compacts at higher temperature could be understood if we consider the phase transformation of ZrO_2 during cooling. Since these Al_2O_3-ZrO_2 composites were prepared from unstabilized ZrO_2, cooling from higher temperature causes spontaneous

t→m phase transformation in ZrO_2. This induces severe micro cracking which probably causes lower observed sintered density. The other factor which might have contributed towards lower sintered density is the presence of chloride ions in the calcined powder since the powders were prepared from the chloride salts of Al and Zr; it is possible that some amount of chloride remain entrapped in the powder itself. It has been observed by others [23] that these entrapped chloride ions adversely affect the sintering behaviour of alumina and zirconia.

3.6 Strength and Hardness

Bending strength of sintered WPT samples was measured in diametral compression test mode and the same is plotted as a function of sintering temperature in Fig.9. The plot shows that bending strength increases with an increase in sintering temperature. The increase in strength is related to the increase in sintered density at higher sintering temperature. Fig.10 shows the semi logarithmic plot of strength vs. volume fraction porosity. The linear variation of log strength with porosity is in accordance with the relation [23].

$$\sigma = \sigma_o \exp(-bp) \qquad (8)$$

The slope of the plot (b) is found to be 3.5 which match well with the reported value. The variation of Vickers hardness with sintering temperature is shown in Fig.11. The plot shows that the hardness increases with an increase in sintering temperature, reaches a value of 4.1 GPa at 1550^0C and subsequently falls to a lower value at 1600^0C. Although the sintered density is higher at 1600^0C, the hardness decreases. Although the sintered density is higher at 1600^0C, cooling from this sintering temperature induces spontaneous tetragonal to monoclinic ZrO_2 transformation. This transformation is associated with

volume expansion which results development of microcracks in the body. The presence of these microcrackes in the samples sintered at 1600^0C, causes the matrix more amenable to indentation.

4. Conclusions

Following conclusions can be drawn from the present study on the effect of powder processing route on phase evolution and densification behaviour of Al_2O_3-ZrO_2 composites:

(1) The three different processing routes adopted viz. Gel-Precipitation, Precipitation and Precipitation followed by hot water and propanol washing has an effect on the crystallization behaviour of Al_2O_3-ZrO_2 composites. While GPT and PPT powders crystallize at 350^0C, no crystallization was observed in WPT powder till 650^0C. Moreover, while GPT powders show a two stage dehydroxylation for $Al(OH)_3$, it was single stage dehydroxylation for both PPT and WPT powders.

(2) WPT powder shows very low agglomerate strength (70MPa) in comparison to GPT (106 MPa) and PPT (97MPa) powders. Thus hot water and propanol washing produces soft agglomerates.

(3) WPT powder has smaller agglomerate size ($d_{0.5}$ = 19μm) which results higher shrinkage (20%) during sintering. All the three powders show a two-stage densification process.

(4) The variation of strength and porosity for the WPT powders show a Semi logarithmic relation.

(5) The Vickers hardness of the WPT samples reaches a maximum value of 4.5 GPa at 1550^0C. At higher sintering temperature (1600^0C), generation of extensive micro cracks reduces the hardness.

Acknowledgement:

References:

1. H. Mills and S. Blackburn.,et al., Zirconia toughened aluminas by hydro-thermal processing, J. Eur. Soc. 20 (2000) 1085-1090.

2. A. Bleier. and C.G. Westmoreland, et al., Effects of pH and particle size on the processing of and the development of microstructure in alumina–zirconia composites, J. Am. Ceram. Soc. 74 (1991) 3100-11.

3. T Suzuki, Y Sakka., K Nakano and H. Hiraga, Effect of ultrasonication on colloidal dispersions of Al_2O_3 and ZrO_2 in pH controlled suspensions, JIM 39 (1998) 682-689.

4. A. Bleier, P.F.Becher, C.G Westmoreland and K.B.Alexander,et al, Effect of aqueous processing conditions on the microstructure and transformation behavior in Al_2O_3 ZrO_2 (CeO_2) composites, J. Am. Ceram. Soc.75 (1992) 2649-58.

5. R.C.Garvie,et al., Occurrence of metastable tetragonal zirconia as a crystallite size effect, J. Phys. Chem. 69 (1965) 1238-43.

6. D Casellas, M.M. Nagl, L Llanes and M Anglada.et al., Fracture toughness of alumina and ZTA ceramics: microstructural coarsening effects, J. Mat. Proc. Tech.143-144 (2003) 148-52.

7. V. S. Vladimir and L. Radonji,et al., Transformation toughening in sol--gel-derived alumina-zirconia composites, J. Am. Ceram. Soc., 80 (1997) 2056-60.

8. T.S Aruna and K.S.Rajam,et al., Mixture of fuels approach for the solution combustion synthesis of Al_2O_3–ZrO_2 nanocomposite, Mat.Res.Bull. 39 (2004) 157-67.

9. S Kikkawa., A. Kijima, K Hirota and O. J. Yamamato,et al., Crystal structure of zirconia prepared with alumina by coprecipitation, J. Am. Ceram. Soc.85 (2002) 721-23.

10. S. Bhattacharyya, S. K.Pratihar, R. K.Sinha, R.C.Behera and R.I.Ganguly, et al., Preparation of alumina–high zirconia microcomposite by combined gel-precipitation, Mat. Lett. 53 (2002) 425-31.

11. O. Vasylkiv and Y. J Sakka,et al., Synthesis and colloidal processing of zirconia nanopowder, J. Am. Ceram. Soc.84 (2001) 2489-94.

12. M. Balasubramanian, S.K. Malhotra and C.V.Gokularathnam,et al., Sintering and mechanical properties of sol-gel derived alumina-zirconia composites, J. Mat. Proc. Tech. 67 (1997) 67-70.

13. M.A.C.G.Van de Graff and A.J. Burggraaf, in: N.Claussen and A.H. Heuer (Eds.), Advances in Ceramics Vol.12., The American Ceramic Society, OH, 1984, pp. 744-765.

14. C.Schmid and O.Sbaizero,et al., Ultrasonic homogenization of equivolumetric Al_2O_3-ZrO_2 suspensions, J. Mat. Sci. 35 (2000) 1213-17.

15. L.Rakotoson and M. Paulus, in: N.Claussen and A.H. Heuer (Eds.), Advances in Ceramics Vol.12, The American Ceramic Society, OH, 1984, pp. 727-32.

16. R. P Rana., S. K.Pratihar and S Bhattacharyya.,et al., Effect of powder treatment on the crystallization behaviour and phase evolution of Al_2O_3-high ZrO_2 nanocomposites, J. Mat. Sci. (in press)

17. Klug, H. and Alexander, L.E., in "X-ray diffraction procedures for polycrystalline and amorphous materials" (John Wiley and Sons, New York, 1974) p. 618-708.

18. D.K.Shetty, A.R Rosenfield and D.H.Duckworth,et al., Mixed-mode fracture of ceramics in diametral compression, J. Am. Ceram. Soc. 69 (1986) 437-443.

19. H. K.Schmid,et al., Quantitative analysis of polymorphic mixes of zirconia by X-ray diffraction, J. Am. Ceram. Soc. 70 (1987) 367-376.

20. E Karapetrova, R.Platzer, E Gardner, E. Torne, J. A.Sommers and W. E.Evenson, Oxygen vacancies in pure tetragonal zirconia powders: dependence on the presence of chlorine during processing, J. Am. Ceram. Soc. 84 (2001) 65-70.

21. R.A. Dimilia and J. S. Reed, Stress Transmission During the Compaction of a Spray-Dried Alumina Powder in a Steel Die, J. Am. Ceram. Soc., 66 (1983) 667-72.

22. J.L.Shi, J.H.Gao, B. S.Li and T.S Yen,et al., Processing of nano-Y-TZP/Al_2O_3 composites.II: compaction and sintering behaviour of nano-Y-TZP/ Al_2O_3 composite powders, J. Euro. Ceram. Soc.15 (1995) 967-73.

23. R.W.Rice, in: R. K MacCrone (Eds) Microstructure dependence of mechanical behaviour of ceramics, Treatise on Materials Science and Technology, Vol.11, Properties and microstructure, New York, SanFrancisco, London: Academy Press 1977, PP. 199-381.

List of Figures

Fig.1 DSC/TG of gel powders: (a) GPT, (b) PPT and (c) WPT.

Fig.2 XRD of calcined GPT powders as a function of calcination temperature.

Fig.3 XRD of calcined PPT powders as a function of calcination temperature.

Fig.4 XRD of calcined WPT powders as a function of calcination temperature.

Fig.5 Particle size distribution of calcined powders.

Fig.6 Compaction behaviour of calcined powders.

Fig.7 Non-isothermal densification behaviour.

Fig.8 Relative density as a function of sintering temperature.

Fig.9 Bending strength as a function of sintering temperature.

Fig.10 Bending strength as a function of porosity.

Fig.11 Hardness as a function of sintering temperature and porosity.
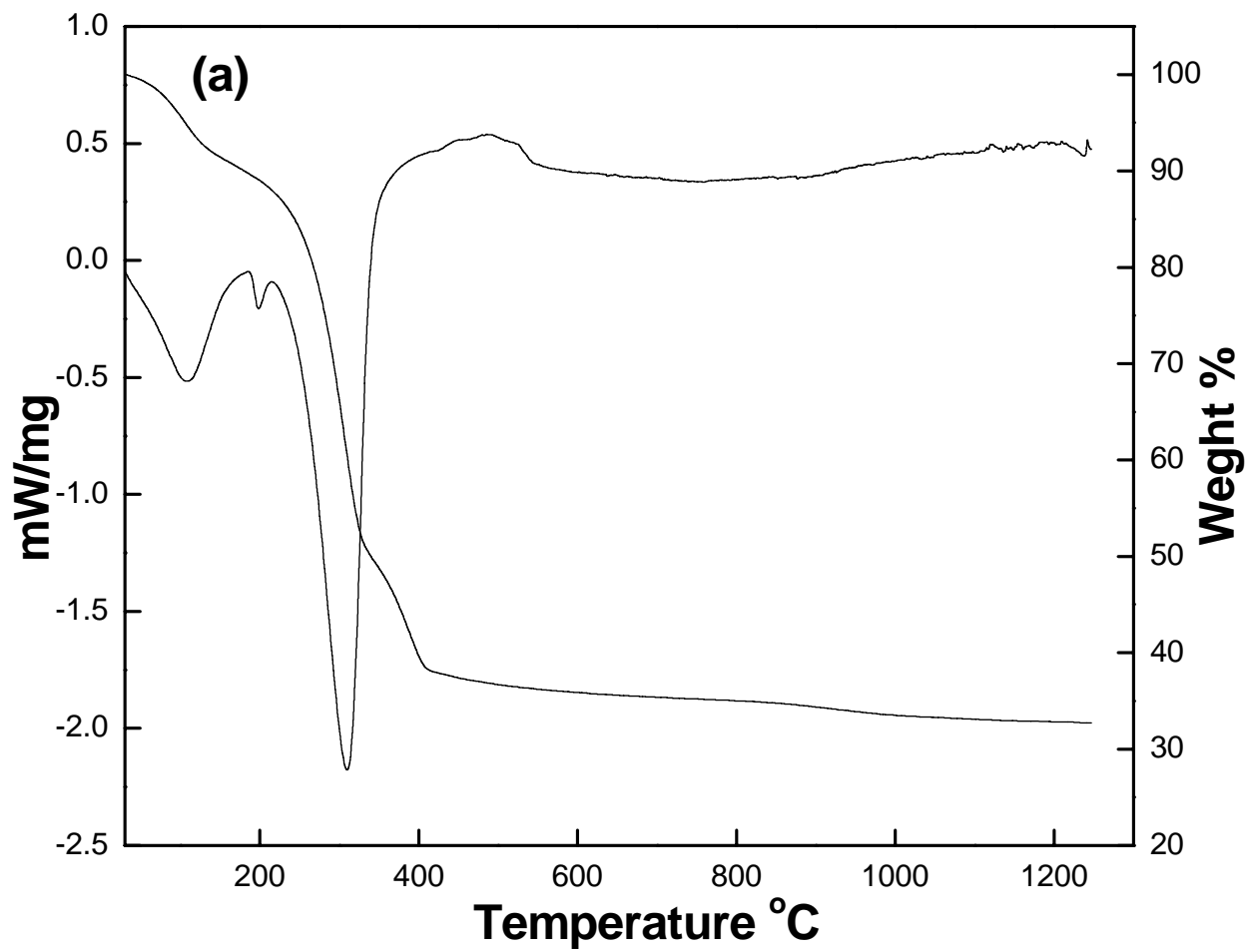
Fig.1 R. P. Rana et. al.
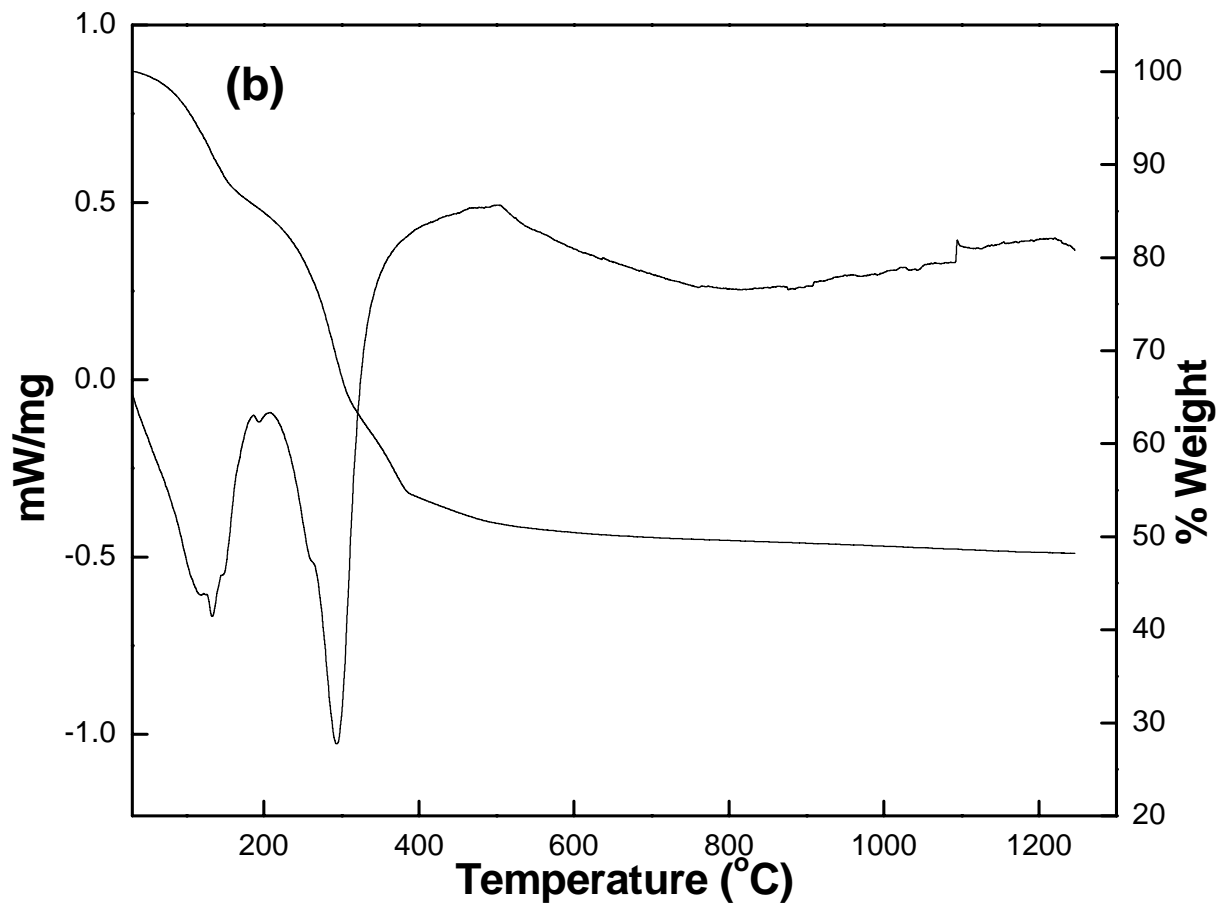
Fig.1 R. P. Rana et. al.
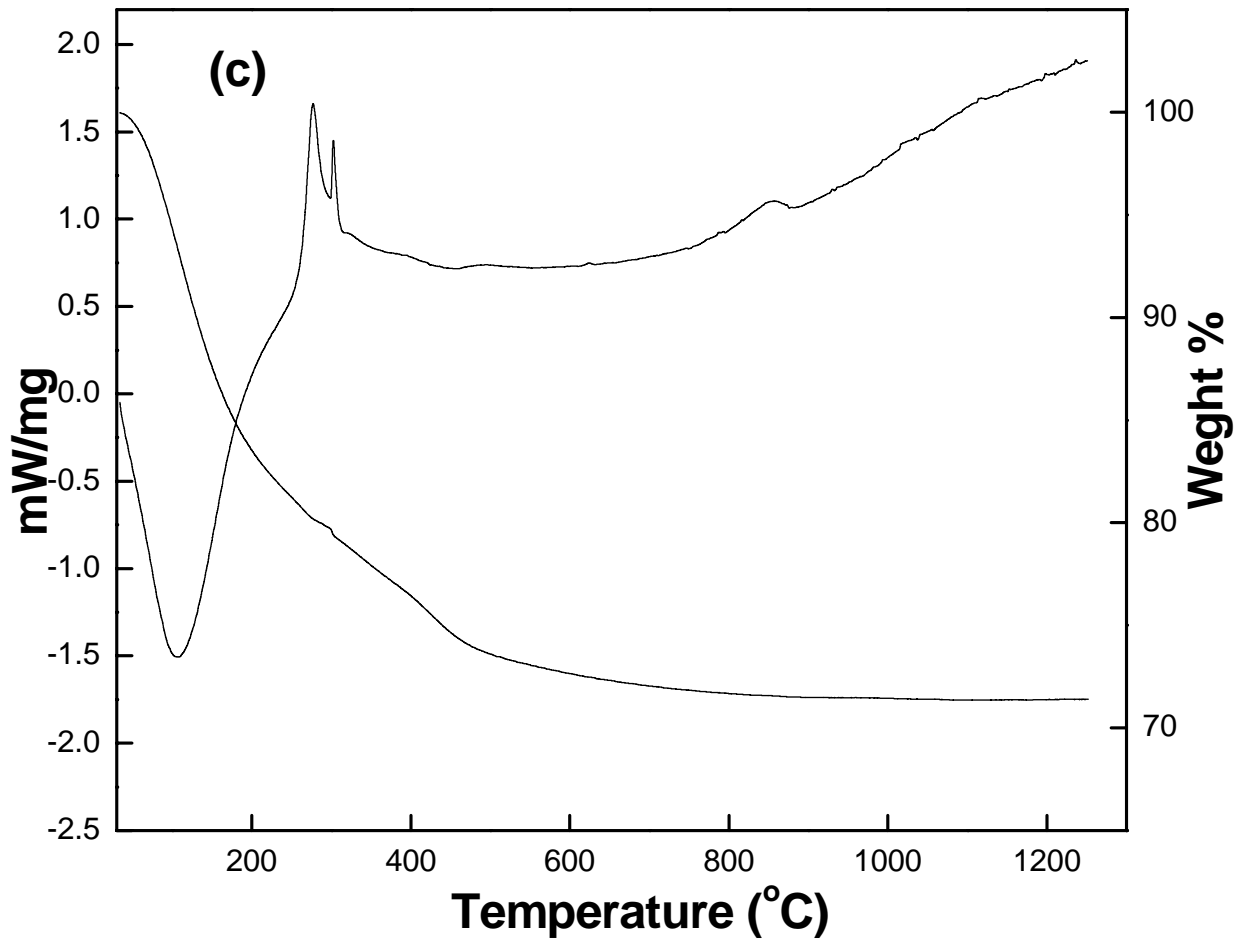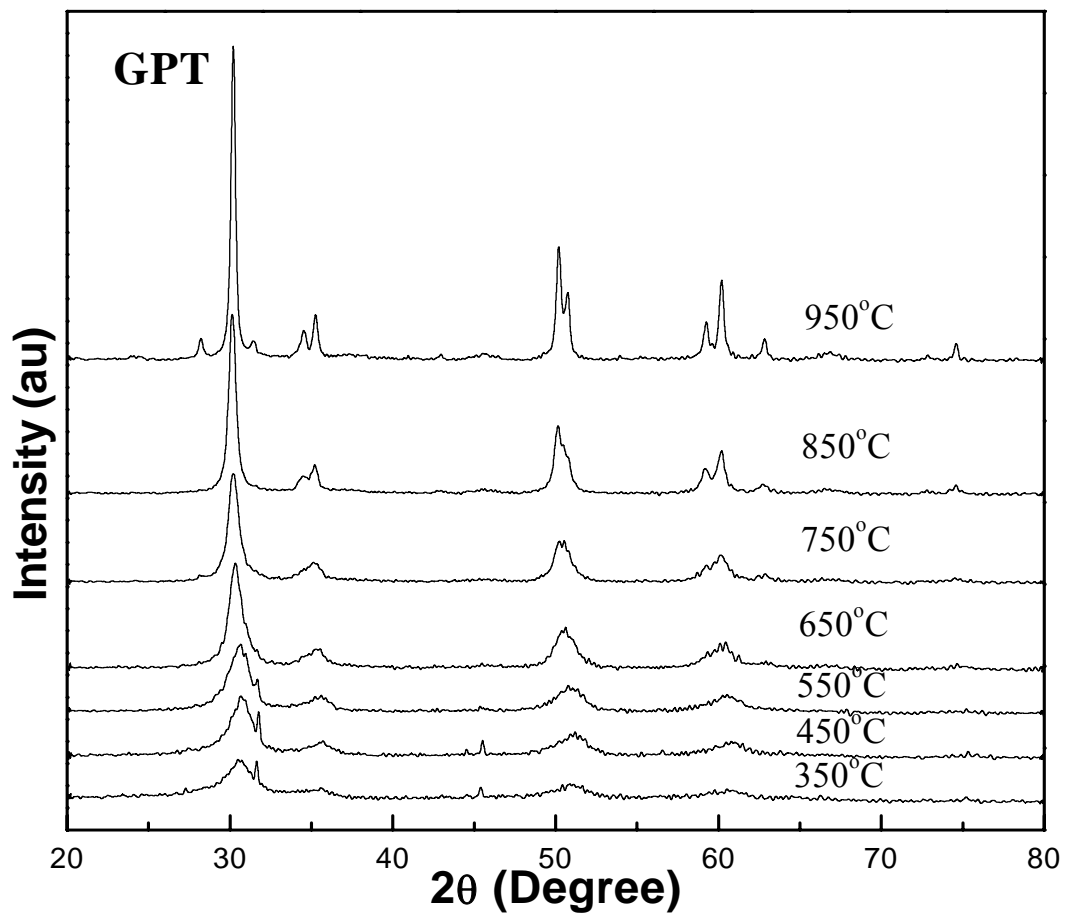
Fig.1R. P. Rana et. al.

Fig.2 R. P. Rana et. al.
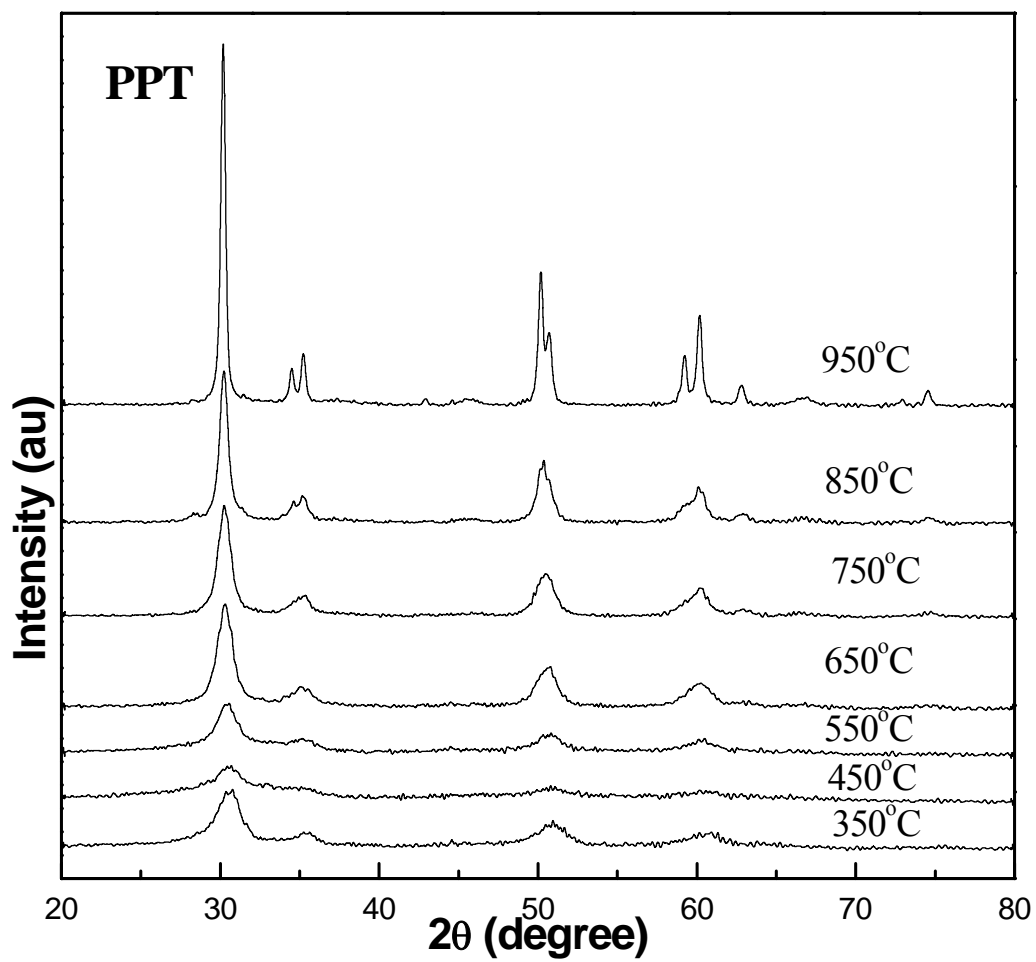
Fig.3 R. P. Rana et. al.
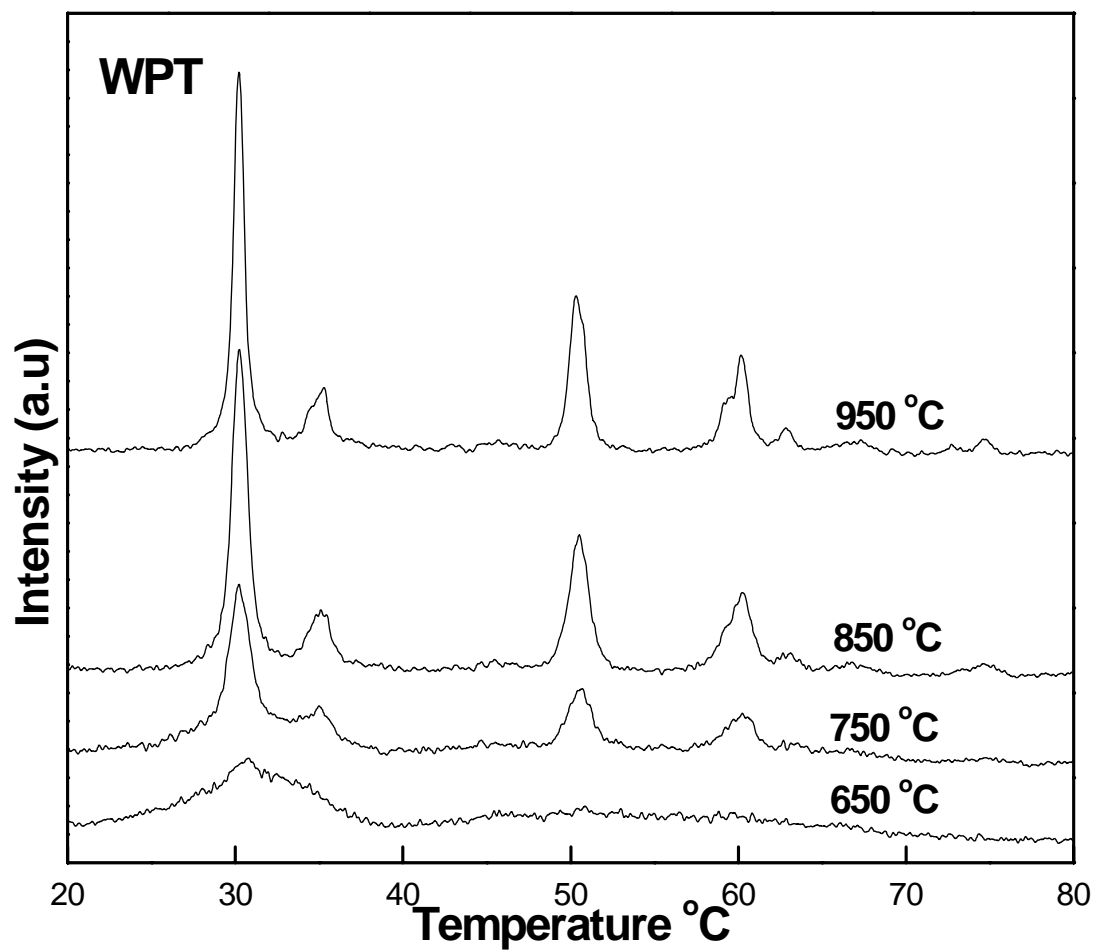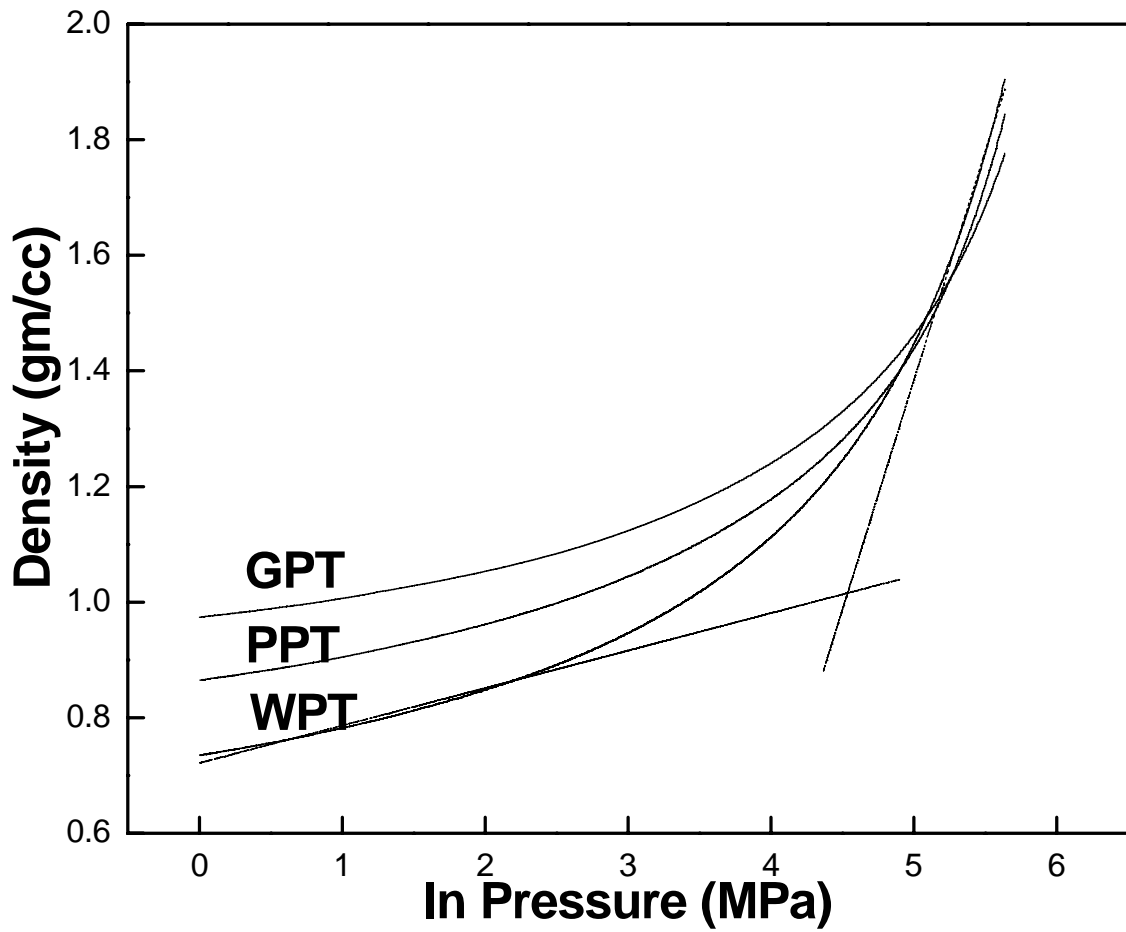
Fig.4 R. P. Rana et. al.
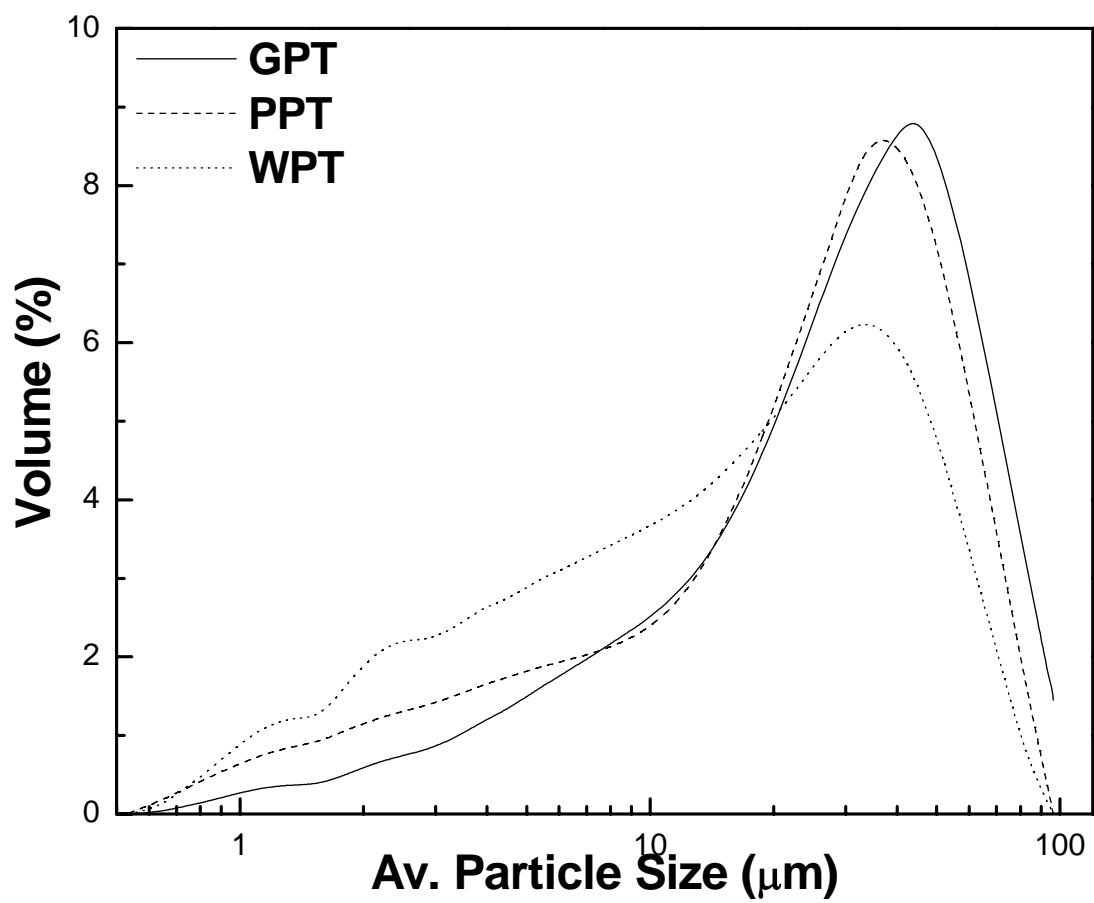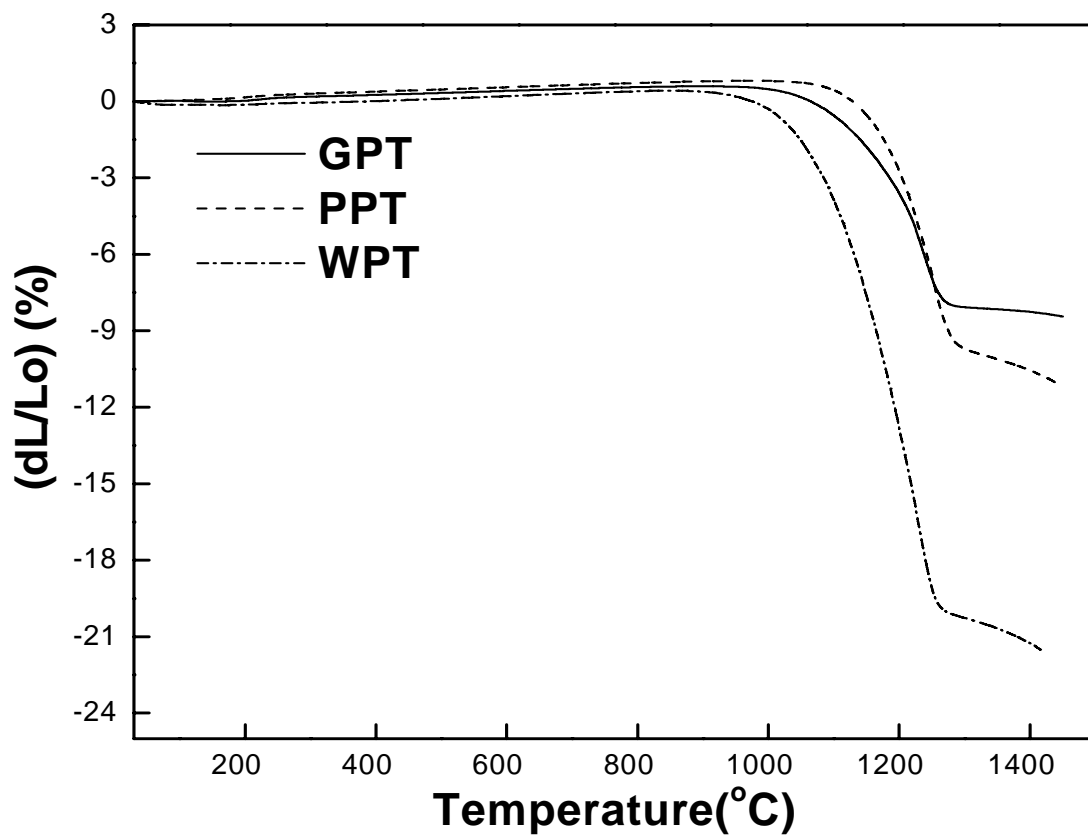
Fig.5 R. P. Rana et. al.
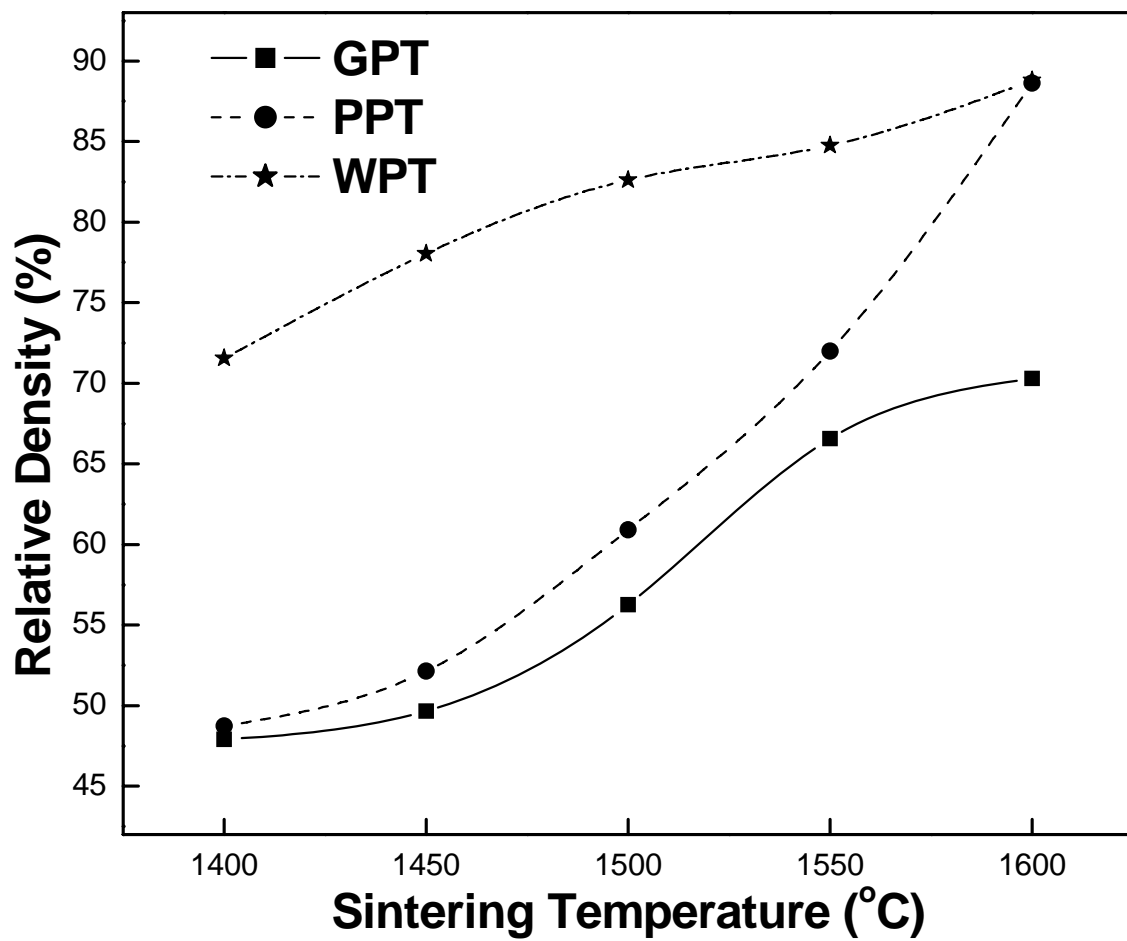
Fig.6 R. P. Rana et. al.
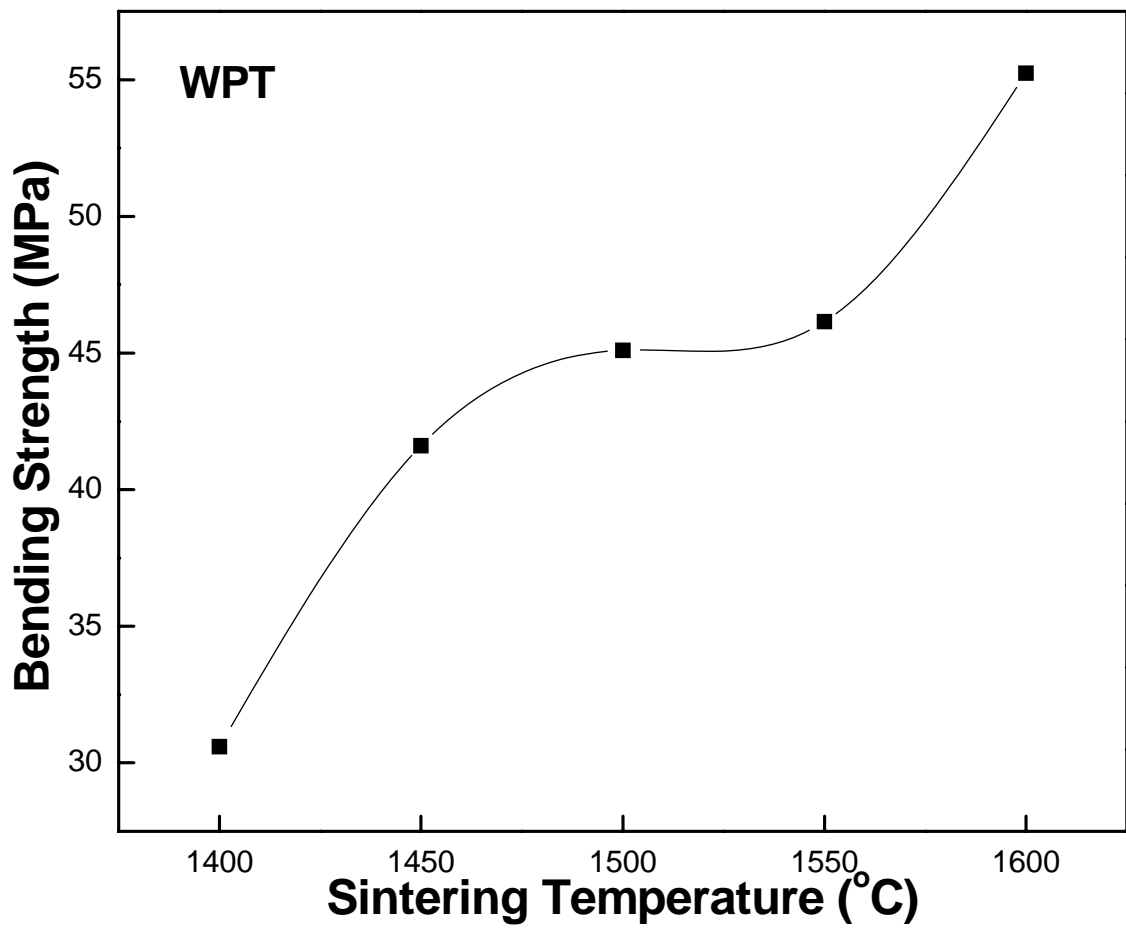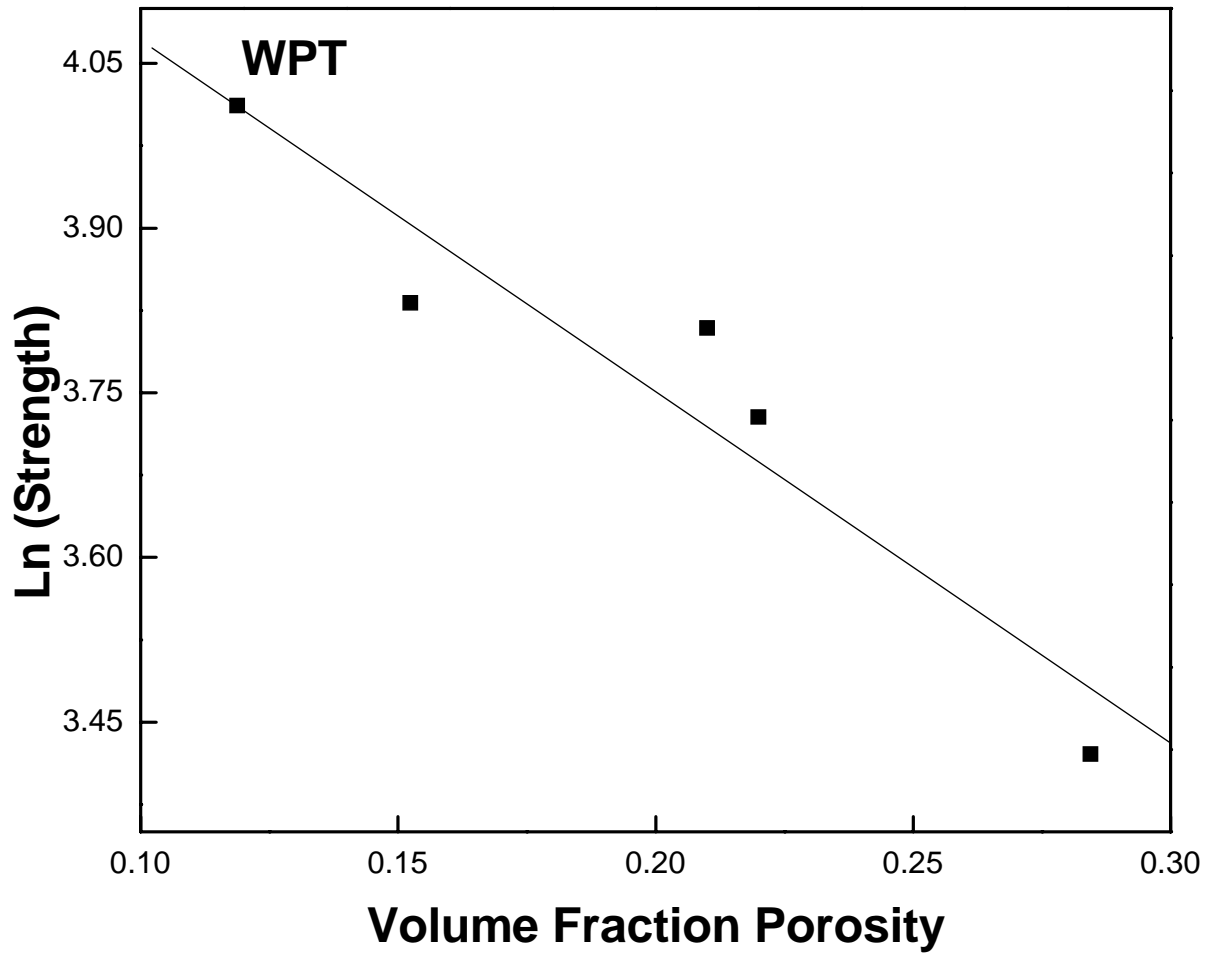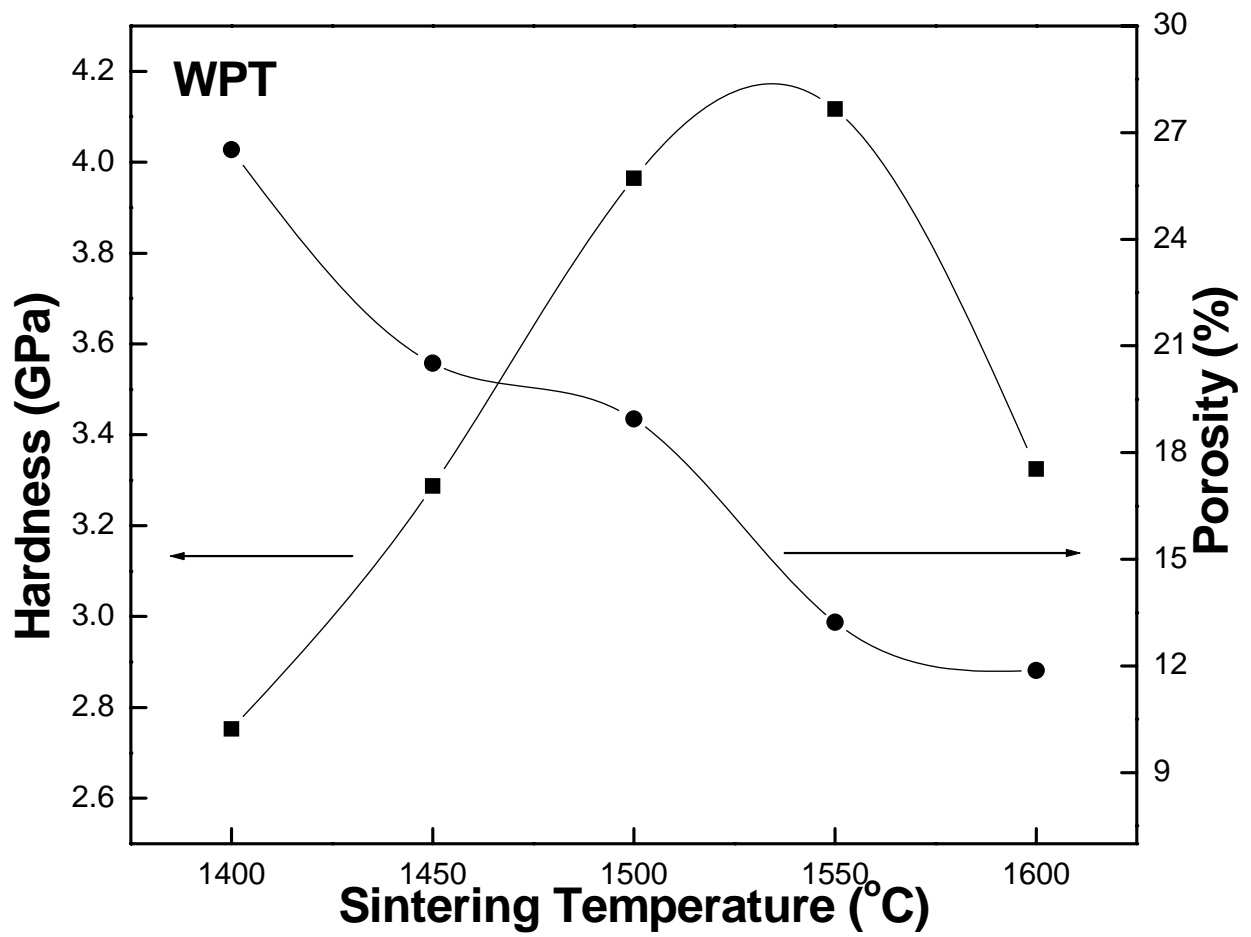
Fig.7 R. P. Rana et. al.

Fig.8 R. P. Rana et. al.

Fig.9 R. P. Rana et. al.

Fig.10 R. P. Rana et. al.

Fig.11 R. P. Rana et. al.